

Magnetism, heat capacity, magnetocaloric effect, and magneto-transport properties of heavy fermion antiferromagnet CeGaSi

Li-Bo Zhang(张黎博), Qing-Xin Dong(董庆新), Jian-Li Bai(白建利), Qiao-Yu Liu(刘乔宇), Jing-Wen Cheng(程靖雯), Cun-Dong Li(李存东), Pin-Yu Liu(刘品宇), Ying-Rui Sun(孙英睿), Yu Huang(黄宇), Zhi-An Ren(任治安), and Gen-Fu Chen(陈根富)

Citation: Chin. Phys. B, 2024, 33 (**6**): 067101. DOI: 10.1088/1674-1056/ad3060
Journal homepage: http://cpb.iphy.ac.cn; http://iopscience.iop.org/cpb

What follows is a list of articles you may be interested in

Electronic structure study of the charge-density-wave Kondo lattice $CeTe_3$

Bo Wang(王博), Rui Zhou(周锐), Xuebing Luo(罗学兵), Yun Zhang(张云), and Qiuyun Chen(陈秋云)
Chin. Phys. B, 2023, 32 (**9**): 097103. DOI: 10.1088/1674-1056/acb41e

$CeAu_2In_4$: A candidate of quasi-one-dimensional antiferromagnetic Kondo lattice

Meng Lyu(吕孟), Hengcan Zhao(赵恒灿), Jiahao Zhang(张佳浩), Zhen Wang(王振), Shuai Zhang(张帅), and Peijie Sun(孙培杰)
Chin. Phys. B, 2021, 30 (**8**): 087101. DOI: 10.1088/1674-1056/ac0a60

Possible nodeless $s^{\pm}$-wave superconductivity in twisted bilayer graphene

Zhe Liu(刘哲), Yu Li(李宇), Yi-Feng Yang(杨义峰)
Chin. Phys. B, 2019, 28 (**7**): 077103. DOI: 10.1088/1674-1056/28/7/077103

Global phase diagram of a spin-orbit-coupled Kondo lattice model on the honeycomb lattice

Xin Li(李欣), Rong Yu(俞榕), Qimiao Si
Chin. Phys. B, 2019, 28 (**7**): 077102. DOI: 10.1088/1674-1056/28/7/077102

Heavy fermions in high magnetic fields

M Smidman, B Shen(沈斌), C Y Guo(郭春煜), L Jiao(焦琳), X Lu(路欣), H Q Yuan(袁辉球)
Chin. Phys. B, 2019, 28 (**1**): 017106. DOI: 10.1088/1674-1056/28/1/017106

Magnetism, heat capacity, magnetocaloric effect, and magneto-transport properties of heavy fermion antiferromagnet CeGaSi

Li-Bo Zhang(张黎博)[1,2], Qing-Xin Dong(董庆新)[1,2], Jian-Li Bai(白建利)[1,2], Qiao-Yu Liu(刘乔宇)[1,2], Jing-Wen Cheng(程靖雯)[1,2], Cun-Dong Li(李存东)[1,2], Pin-Yu Liu(刘品宇)[1,2], Ying-Rui Sun(孙英睿)[1,2], Yu Huang(黄宇)[1,2], Zhi-An Ren(任治安)[1,2], and Gen-Fu Chen(陈根富)[1,2,3,†]

[1] *Institute of Physics and Beijing National Laboratory for Condensed Matter Physics, Chinese Academy of Sciences, Beijing* 100190, *China*
[2] *School of Physical Sciences, University of Chinese Academy of Sciences, Beijing* 100049, *China*
[3] *Songshan Lake Materials Laboratory, Dongguan* 523808, *China*

(Received 22 February 2024; revised manuscript received 4 March 2024; accepted manuscript online 6 March 2024)

We synthesize high-quality single crystal of CeGaSi by a Ga self-flux method and investigate its physical properties through magnetic susceptibility, specific heat and electrical resistivity measurements as well as high pressure effect. Magnetic measurements reveal that an antiferromagnetic order develops below $T_m \sim 10.4$ K with magnetic moments orientated in the *ab* plane. The enhanced electronic specific heat coefficient and the negative logarithmic slope in the resistivity of CeGaSi indicate that the title compound belongs to the family of Kondo system with heavy fermion ground states. The max magnetic entropy change $-\Delta S_M^{max}$ ($\mu_0 H \perp c$, $\mu_0 H = 7$ T) around T_m is found to reach up to 11.85 J·kg^{-1}·K^{-1}. Remarkably, both the antiferromagnetic transition temperature and $-\ln T$ behavior increase monotonically with pressure applied to 20 kbar (1 bar = 10^5 Pa), indicating that much higher pressure will be needed to reach its quantum critical point.

Keywords: heavy fermion, antiferromagnetic order, magnetocaloric effect

PACS: 71.27.+a, 75.30.Sg, 75.30.Gw, 71.20.Eh **DOI:** 10.1088/1674-1056/ad3060

1. Introduction

In recent years, the *RAlX* (*R* = rare earth; *X* = Si, Ge) series of compounds derived from alloys RAl_xSi_{2-x} or RAl_xGe_{2-x}, as the candidates for magnetic topological Weyl semimetals, have attracted considerable attention because they have neither inversion nor time-reversal symmetry, which offers a rare platform to explore exotic quantum phenomena arising from the interplay between magnetism and topology.[1–7] For instance, a singular angular magnetoresistance (AMR), arising from the momentum space mismatching across real space domains and highly tied to principal symmetry directions, was observed in single-crystalline CeAlGe.[5] A novel type of quantum oscillations has also been detected in the temperature dependent electrical resistivity, specific heat, Seebeck and Nernst coefficients under a constant magnetic field in NdAlSi, which was considered to arise from the destructive interference between quantum oscillations from the spin-splitting of Fermi surface due to the strong Weyl fermions–f electrons exchange interaction.[7,8]

Remarkably, the *RAlX* system offers significant material tunability. Replacing Al with Ga makes it very easy to obtain *R*GaSi from RGa_xSi_{2-x} alloys. The properties of these compounds have also been extensively studied, particularly for the polycrystalline samples.[9–13] For example, $CeGa_xSi_{2-x}$ series of compounds demonstrate magnetic properties that are easily adjustable, possibly due to a strong competition between the Ruderman–Kittel–Kasuya–Yosida (RKKY) interactions and Kondo effect.[9,14] In the region $0.7 \leq x \leq 1.3$, the relative intensity of RKKY interactions and Kondo effect changes with x increasing, resulting in a transition from a ground state that is RKKY-dominated to one that is Kondo-dominated. Such an easily adjustable behavior enables the $CeGa_xSi_{2-x}$ series of compounds to exhibit a wide range of physical properties. To date, however, only few studies have been performed on the single crystals.[15]

In this work, we successfully grow the high-quality single crystal of CeGaSi and its non-f reference compound LaGaSi, and systematically study their physical properties. Magnetic and specific heat measurements on CeGaSi unveil an antiferromagnetically ordered state below $T_m = 10.4$ K. Especially, the Ce moment undergoes a metamagnetic transition at different temperatures and magnetic field directions, reflecting a strong magnetic anisotropy. A large magnetocaloric effect (MCE) ($-\Delta S_M^{max} = 11.85$ J·kg^{-1}·K^{-1}, $\mu_0 H = 7$ T), almost twice those of other Ce-based materials with the same structure, can be observed. The resistivity and specific heat data reveal comparable energy scales for the RKKY interactions and Kondo effect. The monotonic enhancement of the Kondo effect and magnetic ordering temperature under applied pressure up to 20 kbar, indicate that much higher pressure is needed to drive

†Corresponding author. E-mail: gfchen@iphy.ac.cn
© 2024 Chinese Physical Society and IOP Publishing Ltd

a quantum phase transition.

2. Experiment details

Single crystals of CeGaSi and LaGaSi were synthesized by the self-flux method.[15] High purity Ce/La (3N), Ga (6N), and Si (4N), in a molar ratio of 1:7:2, were placed in an alumina crucible and sealed into a quartz tube under high vacuum. The sealed quartz tube was heated to 1100 °C in 10 h, held there for 24 h and then cooled to 500 °C at a rate of 6 °C per hour. At this temperature, the liquid flux was removed by centrifugation. A small amount of Ga metal was still attached to the surface of some samples, which could be removed by a short soaking in dilute hydrochloric acid.

Crystal structure was characterized by x-ray diffraction using Cu-$K\alpha$ (wavelength $\lambda = 1.5418$ Å) radiation with a PAN-analytical x-ray diffractometer at room temperature and was analyzed by using the Rietveld method with GSAS-EXPGUI software. The chemical composition was analyzed by an energy dispersive x-ray spectrometer (EDS) equipped on a Phenom scanning electron microscope (SEM) operated at 15 kV. Magnetic property measurements were carried out by using a commercial Quantum Design vibrating sample magnetometer (VSM-7T). Electrical transport properties and specific heat measurements were performed on a commercial Quantum Design physical property measurement system (PPMS). A hybrid CuBe/NiCrAl pressure cell and pressure-medium of daphne 7373 were used to achieve hydrostatic pressure up to 20 kbar for the electrical resistivity measurements under applied pressure.

3. Results and discussion

Figure 1(a) shows the structure of CeGaSi which crystallizes into a tetragonal structure with the space group $I4_1/amd$ (α-$ThSi_2$ type). For this structure, Ga and Si equally populate the positions of each other. The obtained single crystal is plate-like with a size of about 1.2 mm×0.8 mm×0.1 mm as shown in Fig. 1(b). X-ray scans reveal that the naturally grown single-crystalline plate has facets perpendicular to the [001] direction as shown in Fig. 1(c). The lattice parameters, determined from the powder x-ray data (not presented here), $a = 4.239$ Å, $c = 14.14$ Å, are in good agreement with previous results.[9] The EDS analysis yields an atom molar ratio, Ce:Ga:Si = 0.98:1:1.02, consistent with the formula CeGaSi.

In order to explore the magnetism of CeGaSi, temperature dependence of magnetic susceptibility $\chi(T)$ was measured in zero-field-cooling (ZFC) mode and field-cooling (FC) mode under magnetic field ($\mu_0 H = 0.1$ T) perpendicular (the left axis) and parallel (the right axis) to the c axis, respectively as shown in Fig. 1(d). Evidently, the susceptibility is highly anisotropic. For $\mu_0 H \perp c$, both $\chi(T)_{\rm ZFC}$ and $\chi(T)_{\rm FC}$ curves exhibit an increase with temperature decreasing initially at relatively high temperature. Below 10.4 K, $\chi(T)_{\rm ZFC}$ curve and $\chi(T)_{\rm FC}$ curve show a noticeable deviation from each other, with the $\chi(T)_{\rm ZFC}$ curve peaking sharply. For $\mu_0 H \parallel c$, $\chi(T)_{\rm ZFC}$ and $\chi(T)_{\rm FC}$ curves also deviate from each other at low temperature. Both $\chi(T)_{\rm ZFC}$ curve and $\chi(T)_{\rm FC}$ curve deflect at 10.4 K. Clearly, CeGaSi undergoes a magnetic transition at $T_{\rm m} = 10.4$ K and exhibits a strong magnetic anisotropy.

The inverse magnetic susceptibility $1/\chi$ as a function of temperature is plotted in the inset of Fig. 1(d). We fit the data within a temperature range of 150 K–300 K by using the Curie–Weiss law $\chi = C/(T - \theta_{\rm p})$ (C is the Curie constant and $\theta_{\rm p}$ is the Weiss temperature). The values of effective magnetic moment $\mu_{\rm eff}$ are estimated at 2.51 $\mu_{\rm B}$ and 2.54 $\mu_{\rm B}$ for $\mu_0 H \perp c$ and $\mu_0 H \parallel c$, respectively. These values are close to the theoretical free magnetic moment of the Ce^{3+} ion, 2.54 $\mu_{\rm B}$, indicating the presence of well localized cerium magnetic moment. The derived Weiss temperatures are $\theta_{\rm p} = 6.91$ K and $\theta_{\rm p} = -26.01$ K, respectively. Below 150 K, both curves of $1/\chi$ deviate from linear fittings, which should be caused by the crystal electric field (CEF) effect and will be further discussed later.

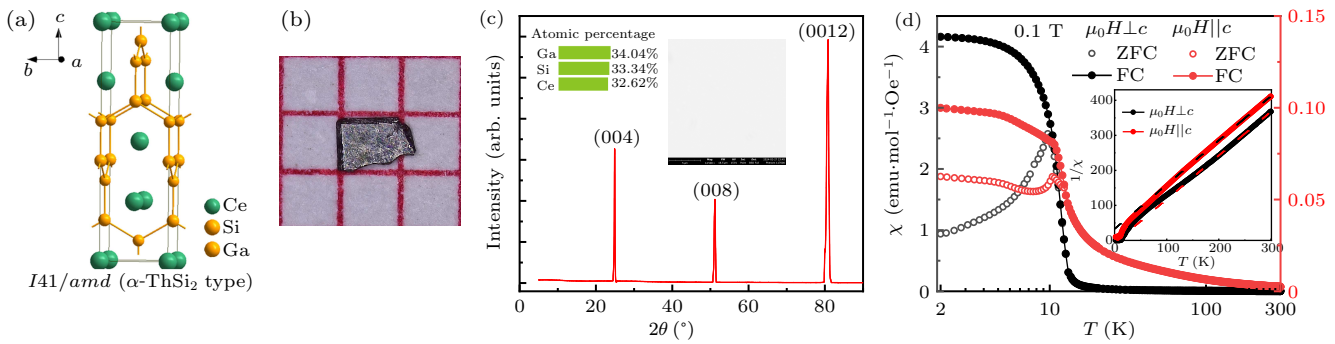


Fig. 1. (a) Schematic diagram for structure of CeGaSi. (b) Picture of single-crystalline CeGaSi. (c) The x-ray diffraction pattern of single-crystalline CeGaSi, with inset showing SEM image and molar ratio from EDS. (d) Temperature dependence of magnetic susceptibility $\chi(T)$, measured in ZFC mode and FC mode under magnetic field $\mu_0 H = 0.1$ T perpendicular (the left axis) and parallel (the right axis) to the c axis, respectively, with inset showing inverse magnetic susceptibility $1/\chi$ measured under magnetic field $\mu_0 H = 0.1$ T, and red and black dashed lines representing Curie–Weiss fittings for $\mu_0 H \perp c$ and $\mu_0 H \parallel c$, respectively. The unit 1 Oe = 79.5775 A·m^{-1}.

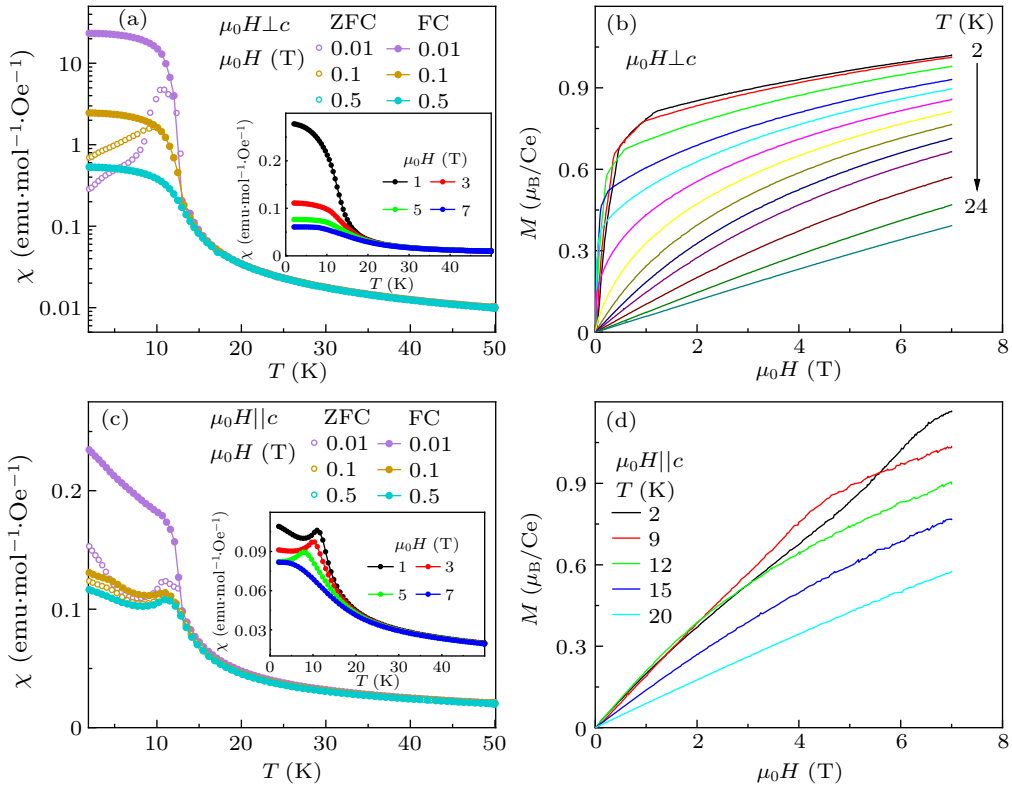


Fig. 2. (a) Curves of $\chi(T)$ versus T measured in ZFC mode and FC mode under different magnetic fields for $\mu_0H\perp c$, with inset showing T-dependent $\chi(T)$ curves measured under different magnetic fields for $\mu_0H\perp c$. (b) Curves of $M(H)$ versus $\mu_0H\perp c$ measured at different temperatures (T = 2, 5, 8, 10, 11, 12, 13, 14, 15, 16, 18, 21, 24 K). (c) Curves of $\chi(T)$ measured in ZFC mode and FC mode under different magnetic fields for $\mu_0H \parallel c$, with inset showing $\chi(T)$ measured under magnetic fields for $\mu_0H \parallel c$. (d) Curves of $M(H)$ measured at different temperatures (T = 2, 9, 12, 15 K) for $\mu_0H \parallel c$.

To further investigate the magnetic properties of CeGaSi, the values of $\chi(T)$ under different magnetic fields were measured in ZFC mode and FC mode. In the $\mu_0H\perp c$ configuration, as shown in Fig. 2(a), the drop of $\chi(T)_{\rm ZFC}$ below $T_{\rm m}$ is gradually suppressed with increasing magnetic fields and disappears above 0.5 T. Meanwhile, the $\chi(T)_{\rm ZFC}$ and $\chi(T)_{\rm FC}$ curves gradually tend to coincide. As shown in the inset of Fig. 2(a), when the temperature is higher than 1 T, $\chi(T)$ increases with temperature decreasing in ferromagnetic fashion. The $M(H)$ curve measured at 2 K, plotted in Fig. 2(b), deflects at 0.5 T, which may correspond to a metamagnetic transition. With temperature increasing, the deflection moves towards the lower field and disappears at 11 K.

When $\mu_0H \parallel c$ (μ_0H = 0.01 T), as depicted in Fig. 2(c), the $\chi(T)_{\rm ZFC}$ and $\chi(T)_{\rm FC}$ curves diverge at low temperature, and the $\chi(T)_{\rm ZFC}$ curve reaches its peak at $T_{\rm m}$. With the increase of magnetic field, $\chi(T)_{\rm FC}$ curves each exhibit a concurrent decrease at $T_{\rm m}$. At μ_0H = 0.5 T, the $\chi(T)_{\rm ZFC}$ and $\chi(T)_{\rm FC}$ curves overlap and descend below $T_{\rm m}$ in an antiferromagnetic manner. With further increase of magnetic field, spike in the $\chi(T)$ curve shifts towards lower temperatures. The spike of $\chi(T)$ curve is entirely suppressed until the magnetic field reaches 7 T. While for both $\chi(T)_{\rm ZFC}$ curves at 0.01 T with $\mu_0H\perp c$ and $\mu_0H \parallel c$, there is a deflection above $T_{\rm m}$, suggesting the presence of a short-range spin–spin correlations. Figure 2(d) shows $M(H)$ measured at different temperatures with $\mu_0H \parallel c$. At 2 K, $M(H)$ increases linearly under low fields. When magnetic field increases to 6 T, a metamagnetic-like transition appears, corresponding to the bending on the $M(H)$ curve. It is associated with the suppression of the magnetic order, which is also observed in $\chi(T)$ data. With temperature increasing, the bending in $M(H)$ curve moves towards the low magnetic fields and finally disappears at 12 K. The $M(H)$ curves for $\mu_0H \parallel c$ display characteristics indicative of antiferromagnetic interactions. All of these indicate that the present compound is strongly anisotropic and, like other compounds in the material family RAlX, exhibits a rich variety of magnetic states. To elucidate the intricate magnetic structure of CeGaSi, additional studies by using neutron diffraction is necessary.

It is noteworthy that the reported magnetic properties of polycrystalline CeGaSi are quite different from those of single-crystalline CeGaSi. As listed in Table 1, with x increasing from 0 to 2, polycrystalline CeGa$_x$Si$_{2-x}$ undergoes an evolution from non-magnetic to ferromagnetic to antiferromagnetic ground state.[10,11,14,16–18] Especially, the polycrystalline CeGa$_x$Si$_{2-x}$ in a range of $0.7 \le x \le 1$ are ferromagnetical at low temperature.[17] When $x \ge 1.5$, the compounds exhibit an antiferromagnetic ground state.[10] The ferromagnetic-like properties observed in polycrystalline CeGaSi may be attributed to its high anisotropy.

Table 1. Magnetic properties of polycrystalline $CeGa_xSi_{2-x}$. SC: single-crystals, PC: polycrystals, AF: antiferromagnetic, NM: non-magnetic, FM: ferromagnetic.

Materials	Magnetic transitions	T_m (K)	Reference
CeGaSi SC	AF	10.4	this work
$CeSi_2$ PC	NM	–	[18]
$CeGa_{0.7}Si_{1.3}$ PC	FM	10.5	[17]
CeGaSi PC	FM	9	[17]
$CeGa_{1.3}Si_{0.7}$ PC	FM	2.5	[17]
$CeGa_{1.5}Si_{0.5}$ PC	AF	3	[10]
$CeGa_2$ PC	multi-AF	11; 8.5	[16,19]

Based on the $M(H)$ plotted in Figs. 2(b) and 2(d), the magnetic entropy change ΔS_M resulting from the change of magnetic field can be calculated from the following thermodynamic Maxwell relation:[20]

$$\Delta S_M(T,H) = \mu_0 \int_0^H \left(\frac{\partial S}{\partial H}\right)_T \mathrm{d}H = \mu_0 \int_0^H \left(\frac{\partial M}{\partial T}\right)_H \mathrm{d}H. \quad (1)$$

Figures 3(a) and 3(b) show that the $-\Delta S_M$ of CeGaSi is also anisotropic. $-\Delta S_M$ curves for both $\mu_0 H \perp c$ and $\mu_0 H \parallel c$ exhibit sharp peaks near 12 K, with the variation of peak values. For $\mu_0 H \perp c$, $-\Delta S_M$ reaches a maximum value $-\Delta S_M^{max}$, 9.94 J·kg^{-1}·K^{-1} and 11.85 J·kg^{-1}·K^{-1} around T_m for $\mu_0\Delta H =$ 5 T and 7 T, respectively. However, for $\mu_0 H \parallel c$, the values of $-\Delta S_M^{max}$ are only 4.66 J·kg^{-1}·K^{-1} and 6.45 J·kg^{-1}·K^{-1}, respectively. The relative cooling power (RCP) can be calculated from $-\Delta S_M$ by using the following formula:[20]

$$\mathrm{RCP}(\mu_0 H) = |\Delta S_M^{max}(\mu_0 H)| \cdot \delta T_{FWHM}. \quad (2)$$

Here, δT_{FWHM} represents the full width at half maximum of the corresponding $-\Delta S_M^{max}$ curve. The value of RCP can be used to estimate the amount of heat which can be transferred between cold reservoir and hot reservoir. For $\mu_0 H \perp c$, the value of RCP reaches 63.3 J·kg^{-1} for $\mu_0\Delta H = 5$ T and 93.12 J·kg^{-1} for $\mu_0\Delta H = 7$ T. As shown in Fig. 3(c), the RCP increases linearly with the increase of field.

Parameters of MCE for other Ce-based materials are listed in Table 2. It is clear that $-\Delta S_M^{max}$ ($\mu_0 H \perp c$) of single-crystalline CeGaSi is much larger than that of other Ce-based materials with the same structure and is approximately 1/4 that of $ErAl_2$, which is one of the best magnetic refrigerants near 10 K, suggesting potential applications for CeGaSi.

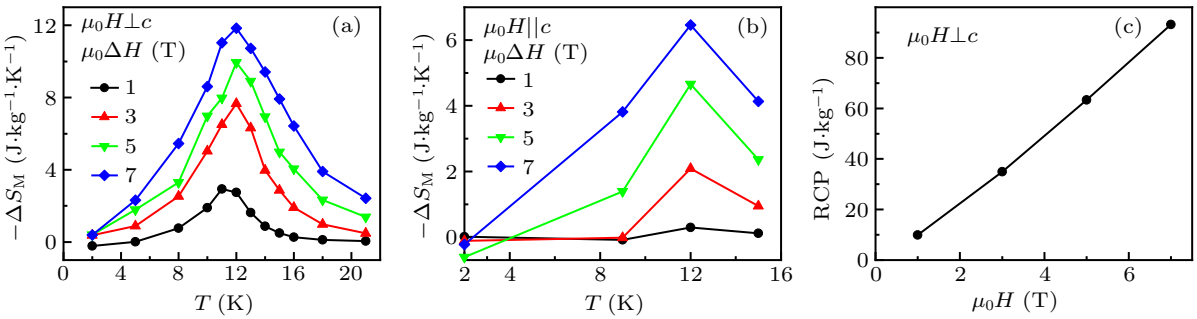


Fig. 3. (a) Magnetic entropy change $-\Delta S_M(T)$ for $\mu_0 H \perp c$. (b) $-\Delta S_M(T)$ for $\mu_0 H \parallel c$. (c) Relative cooling power (RCP) for $\mu_0 H \perp c$.

Table 2. Comparison of MCE between CeGaSi and other Ce-based magnetic materials for $\mu_0\Delta H = 5$ T or 7 T. SC: single-crystals, PC: polycrystals.

Materials	$\mu_0\Delta H$ (T)	T_m (K)	$-\Delta S_M$ (J·kg^{-1}·K^{-1})	RCP (J·kg^{-1})	Reference
CeGaSi SC	5	10.4	9.94	63.3	this work
CeGaSi SC	7	10.4	11.85	93.12	this work
$CeGa_{0.7}Si_{1.3}$ PC	5	10.5	5.7	32.8	[13]
CeAlSi SC	5	5	6	–	[21]
$CeGa_2$ PC	7	10	6.5	–	[22]

Figure 4(a) shows the specific heat divided by temperature, C_p/T versus T^2 of CeGaSi. It is clear that a λ-shaped peak appears at 10.4 K, corresponding to the magnetic transition at T_m. According to the Debye model, the specific heat at low temperatures is described by the following equation:

$$C_p = \gamma T + \beta T^3, \quad (3)$$

where γT and βT^3 denote the contributions of electrons and phonons to the specific heat, respectively. The Debye temperature satisfies the following equation:

$$\Theta_D = \left(12\pi^4 NR/(5\beta)\right)^{1/3}. \quad (4)$$

By fitting the data in a temperature range of 10 K–15 K, the Debye temperature $\Theta_D = 308.1$ K and the specific heat coefficient $\gamma_{Ce} = 83.8$ mJ/(mol·K^2) are obtained. To further investigate the specific heat, single-crystalline LaGaSi with the same structure was also synthesized and its C_p/T versus T^2 in a temperature range of 0 K–15 K is shown in the inset of Fig. 4(a). The fitting below 10 K yields $\gamma_{La} = 2.7$ mJ/(mol·K^2)

and $\Theta_D = 314.6$ K, with the γ_{La} significantly lower than γ_{Ce} and the Θ_D close to that of CeGaSi, which confirms that the two do have the same lattice contribution. Thus, the specific heat of LaGaSi can be treated as a contribution from the lattice to obtain the magnetic contribution to specific heat $C_m = C_{Ce} - C_{La}$, as shown in Fig. 4(b). The magnetic entropy S_m is obtained by integrating C_m/T over T, which is plotted in the inset of Fig. 4(b). The S_m reaches $R\ln 2$ at $T \sim 15$ K, indicating that the ground state of CeGaSi is Kramers two-fold degenerate. According to the Kondo model with a spin of 1/2, the magnetic entropy S_m and Kondo temperature T_K satisfy the following equation:[23,24]

$$S_m(\xi) = R\ln\left[1 + \exp(-\xi) + \xi\frac{\exp(-\xi)}{1+\exp(\xi)}\right]. \quad (5)$$

Here, $\xi = T_K/T_m$. When S_m reaches $0.72R\ln 2$ at $T_m = 10.4$ K, the T_K is estimated at 13.3 K, which is close to T_m, suggesting that the energy scale of the RKKY interaction is comparable to that of the Kondo effect. A broad hump centered around 50 K can be seen in the C_m curve, which is a common feature of Kondo lattice compounds and usually attributed to the CEF effect.[25–28] The Schottky anomaly contribution arising from the CEF effect to the specific heat conforms to the following equation:[27,29]

$$C_{CEF}(T) = \left(\frac{R}{T^2}\right)\left[\sum_i g_i \exp\left(-\frac{\Delta_i}{T}\right)\sum_i g_i\Delta_i^2\exp\left(-\frac{\Delta_i}{T}\right) - \left(\sum_i g_i\Delta_i\exp\left(-\frac{\Delta_i}{T}\right)\right)^2\right] \times\left(\sum_i g_i\exp\left(-\frac{\Delta_i}{T}\right)\right)^2. \quad (6)$$

Here, g_i represents the degeneracy of the i-th excited level with energy separations Δ_i. For Ce^{3+} ion experiencing tetragonal crystal-field potential, we chose the doublet–doublet–doublet scheme with energy separations Δ_1 and Δ_2 to express the Schottky anomaly. The fitting parameters are as follows: $\Delta_1 = 106$ K (~ 9.1 meV) and $\Delta_2 = 149$ K (~ 12.8 meV).

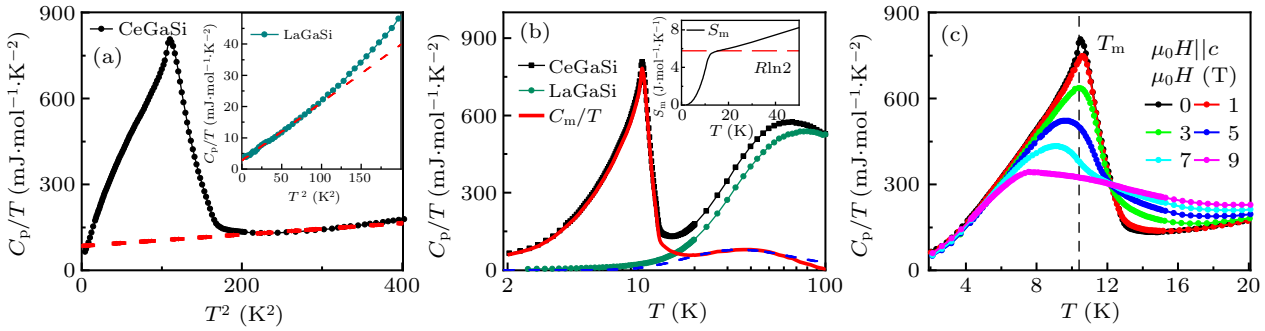


Fig. 4. (a) Specific heat divided by temperature C_p/T versus T^2 of single-crystalline CeGaSi in a temperature range of 0 K–20 K, with inset showing C_p/T versus T^2 of LaGaSi, and red dashed lines representing fittings of C_p/T by Debye model. (b) Curves of C_p/T versus $\log T$ of CeGaSi and LaGaSi in a temperature range between 0 K and 100 K. $C_m/T = C_{Ce}/T - C_{La}/T$, with blue dashed line showing the contribution of the CEF effect, and inset indicating magnetic entropy S_m calculated by integrating C_m/T over T. (c) C_p/T of CeGaSi measured under different magnetic fields for $\mu_0 H \parallel c$ within temperature range of 2 K–20 K.

The values of C_p/T measured under different magnetic fields are shown in Fig. 4(c). As the magnetic field increases, the peaks of the specific heat curves at T_m undergo gradual suppression and significant broadening. At 5 T, a broad hump emerges above the magnetic transition at T_m, which is characteristic of polarized ferromagnetic state. Such a behavior is very common in the antiferromagnetic Ce-based Kondo lattice compounds, such as $CeNiGe_3$[30] and $CeAgAs_2$,[31] which further proves that the transition at T_m is not a simple ferromagnetic transition that can be detected in polycrystalline sample.

Figure 5(a) depicts the curves of resistivity $\rho(T)$ of single-crystalline CeGaSi under various pressures, which is measured by four-probe method with an applied current in *ab* plane. At zero pressure, $\rho(T)$ of CeGaSi decreases with temperature decreasing in a temperature range from 300 K to 200 K and subsequently starts to rise below 200 K. The $\rho(T)$ increases in a minus logarithmic temperature manner in temperature ranges of 50 K–200 K and 10.4 K–20 K, reflecting the Kondo-type scattering.[32] There is a bulge centered around 50 K on the $\rho(T)$ curve, which is caused by the CEF effect.[33,34] Considering the aforementioned data, the temperature regions exhibiting changes caused by the CEF effect in $1/\chi$, $C_m(T)$ and $\rho(T)$ are consistent. Below 10.4 K, the resistivity drops rapidly with temperature decreasing, due to the reduced scattering in the ordered state.

Apparently, the resistivity $\rho(T)$ rises with pressure increasing at a constant temperature. T_m at which the resistivity starts to decline is increasing, suggesting that the RKKY interaction is enhanced with the increase of pressure. Similar behavior was also observed in the isostructural CeAlGe.[35] Meanwhile, the $-\ln T$ behavior in $\rho(T)$ is also enhanced, signifying an enhancement of the Kondo effect in CeGaSi. As is well known, by applying pressure, most of the antiferromagnetic transitions of heavy fermions first increase and then decrease, and finally reach a quantum critical regime.[36] There is no doubt that much higher pressure is demanded to study

the effect of quantum criticality in CeGaSi.

Figure 5(b) shows the angular magnetoresistance $\rho(\theta)$ of CeGaSi. Here, θ represents the angle between $\mu_0 H$ and c axis. Directions of magnetic field rotate in the plane containing the applied current and c axis. $\rho(\theta)$ curves exhibit a period of 180°. When $\mu_0 H \parallel c$ ($\theta = 0°$), $\rho(\theta)$ of CeGaSi reaches a maximum value at 7 T, and then decreases with field increasing, which may be related to the metamagnetic transition at 6 T. When $\mu_0 H \perp c$ ($\theta = 90°$), $\rho(\theta)$ hardly varies with magnetic field. At this point, the material is approaching a fully polarized state, making the change in resistivity with the magnetic field very small.

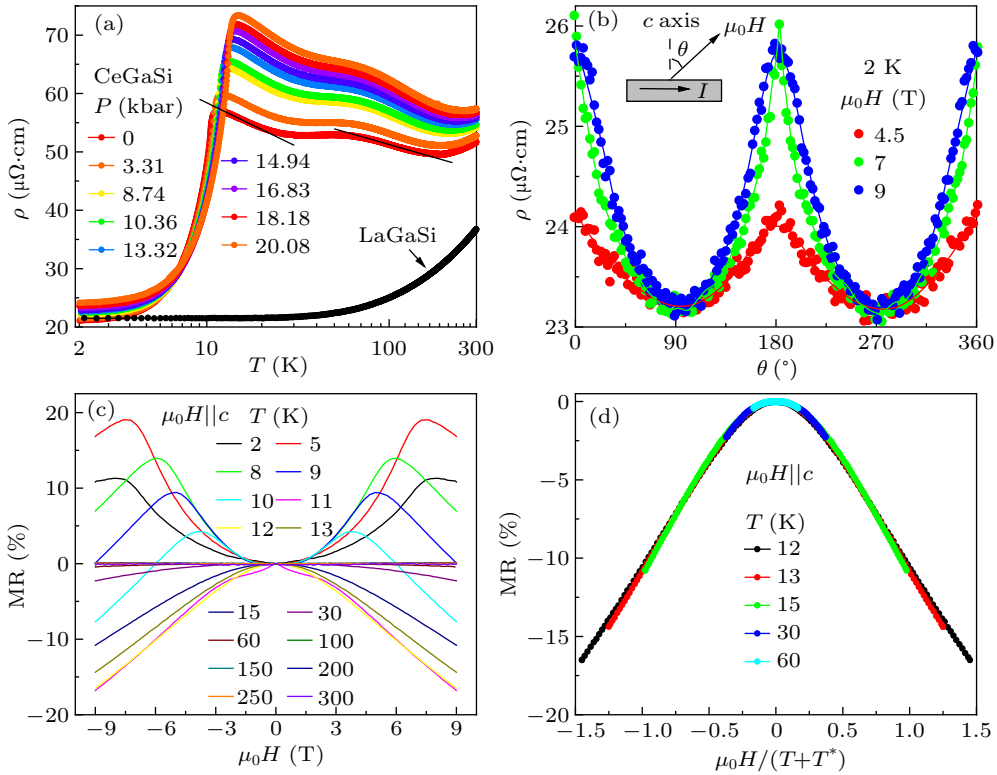


Fig. 5. (a) Plots of resistivity $\rho(T)$ versus $\log T$ of CeGaSi measured under various pressures (pressures from bottom to top are 0, 3.31, 8.74, 10.36, 13.32, 14.94, 16.83, 18.18, and 20.08 kbar (1 bar = 10^5 Pa), respectively) and resistivity $\rho(T)$ versus $\log T$ of LaGaSi under zero pressure, with black lines representing linear fittings to $\log T$. (b) Angular magnetoresistance of CeGaSi at 2 K under different magnetic fields with current in the magnetic field rotation plane. (c) Magnetoresistance MR for $\mu_0 H \parallel c$ and $\mu_0 H \perp I$ measured at several temperatures. (d) MR for $\mu_0 H \parallel c$ and $\mu_0 H \perp I$ as a function of $\mu_0 H/(T + T^*)$ (T^* is the characteristic temperature).

For further study, the curves of field-dependent magnetoresistance MR ($\mu_0 H \parallel c$, $\mu_0 H \perp I$) are measured at several temperatures as shown in Fig. 5(c). Below T_m, MR is positive at low fields. As field increases, MR reaches a maximum and subsequently decreases. Such MR curves are commonly observed in Kondo lattice compounds with antiferromagnetic correlations, like $CeNiGe_3$,[30] Ce_2IrSi_3,[37] and $YbNiAl_2$.[38] Above T_m, MR becomes negative and MR curves at different temperatures exhibit a characteristic Kondo-like shape. These curves conform to equation[39]

$$\mathrm{MR}\,(\mu_0 H) = f[\mu_0 H/(T + T^*)]. \tag{7}$$

Here, T^* represents the characteristic temperature related to Kondo temperature. When T^* is −5.8 K, MR isotherms overlap as shown in Fig. 5(d), indicating the presence of strong ferromagnetic correlations.[30,40]

Figure 6(a) shows the curves of Hall resistivity ρ_{xy} versus $\mu_0 H \parallel c$, measured at various temperatures. In the same field, the absolute value of ρ_{xy} increases with the increase of temperature in a temperature range of 2 K–10 K, followed by a decrease in a temperature range of 11 K–30 K. Such a behavior is typical in Ce-based Kondo lattice compounds and may be attributed to the ordinary Hall effect and residual skew scattering by defects and impurities.[41] Since the field dependence of ρ_{xy} is approximately linear in low fields, the Hall coefficient R_H can be roughly defined as the slope of the ρ_{xy}. As shown in Fig. 6(b), the R_H is almost temperature-independent at high temperatures. While below 100 K, R_H decreases with temperature decreasing, and turns into a sharp dip around T_m. The following equation has been used to fit the R_H data within the high-temperature range ($T \gg T_K$):[42]

$$\begin{aligned} R_H(T) &= R_H^{ord} + \gamma\tilde{\chi}(T)\rho(T) \\ &\quad + [R_H(T=0) - R_H^{ord}]\chi(T)/\chi(T=0). \end{aligned} \tag{8}$$

Here, R_H^{ord} is the ordinary Hall coefficient, $\tilde{\chi}(T) = \chi(T)/C$ (C is the Curie constant), and $\rho(T) = \rho_{Ce}(T) - \rho_{La}(T)$.[42]

The second term on the right-hand in Eq. (8) represents the contribution from intrinsic skew-scattering, and the third term characterizes contribution from the residual scattering by defects and impurities. The γ is the temperature-independent coefficient related to the phase shift.[30] By fitting the data in a temperature range of 100 K–300 K, the parameter $R_{\rm H}^{\rm ord} = 0.019$ μΩ·cm·T^{-1} and $\gamma = -0.485$ K·T^{-1} are derived. The corresponding carrier density is determined as 3.31×10^{22} cm^{-3} under one-band approximation $n = 1/(eR_{\rm H}^{\rm ord})$.

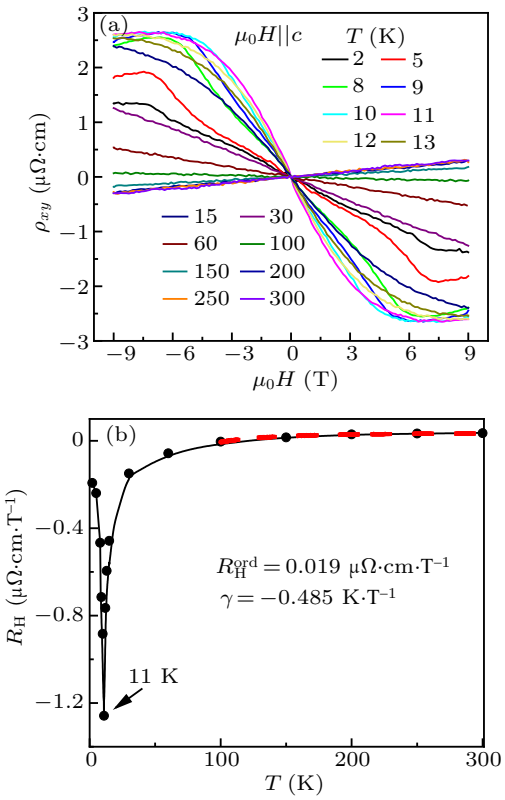


Fig. 6. (a) Curves of field-dependent Hall resistivity ρ_{xy} measured at various temperatures. (b) Curve of temperature-dependent Hall coefficients $R_{\rm H}$, with red dashed line representing fitting of $R_{\rm H}$ to Eq. (8).

4. Conclusions

In this work, we have systematically studied the magnetic, thermodynamic, and electrical transport properties of single-crystalline CeGaSi synthesized by the self-flux method. We find that single crystalline CeGaSi exhibits an antiferromagnetic state instead of the observed ferromagnetism in polycrystalline sample. In order to characterize the magnetic behavior of CeGaSi in more detail, further experimental studies, such as neutron-diffraction investigation, are needed. In addition, the specific heat and electrical resistivity measurements demonstrate that CeGaSi belongs to the family of Kondo systems with heavy fermion ground states. The Kondo temperature $T_{\rm K}$ estimated from the specific heat data is about 13 K. Up to the pressure of 20 kbar, both the Kondo effect and the magnetic ordering temperature are monotonically enhanced, indicating that much higher pressures are needed to suppress the magnetism and expose a quantum phase transition. Furthermore, the magnetic entropy change $-\Delta S_{\rm M}$ around $T_{\rm m} = 10.4$ K for ($\mu_0 H \perp c$, $\mu_0 H = 7$ T) reaches up to 11.85 J·kg^{-1}·K^{-1}, suggesting that CeGaSi is a promising magnetocaloric material with great potential applications in low temperature refrigeration.

Acknowledgements

Project supported by the National Natural Science Foundation of China (Grant No. 12274440), the Strategic Priority Research Program (B) of the Chinese Academy of Sciences (Grant No. XDB33010100), the Fund from the Ministry of Science and Technology of China (Grant No. 2022YFA1403903), and the Fund of the Synergetic Extreme Condition User Facility (SECUF).

References

[1] Chang G, Singh B, Xu S Y, *et al.* 2018 *Phys. Rev. B* **97** 041104
[2] Yang H Y, Singh B, Gaudet J, *et al.* 2021 *Phys. Rev. B* **103** 115143
[3] Yang H Y, Gaudet J, Verma R, Baidya S, Bahrami F, Yao X H, Huang C Y, DeBeer-Schmitt L, Aczel AA, Xu GY, Lin H, Bansil A, Singh B and Tafti F 2023 *Phys. Rev. Mater.* **7** 034202
[4] Wang J F, Dong Q X, Huang Y F, Wang Z S, Guo Z P, Wang Z J, Ren Z A, Li G, Sun P J, Dai X and Chen G F 2023 *Phys. Rev. B* **108** 024423
[5] Puphal P, Pomjakushin V, Kanazawa N, Ukleev V, Gawryluk D J, Ma J, Naamneh M, Plumb N C, Keller L, Cubitt R, Pomjakushina E and White J S 2020 *Phys. Rev. Lett.* **124** 017202
[6] Hodovanets H, Eckberg C J, Zavalij P Y, Kim H, Lin W C, Zic M, Campbell D J, Higgins J S and Paglione J 2018 *Phys. Rev. B* **98** 245132
[7] Wang J F, Dong Q X, Guo Z P, Lv M, Huang Y F, Xiang J S, Ren Z A, Wang Z J, Sun P J, Li G and Chen G F 2022 *Phys. Rev. B* **105** 144435
[8] Dong Q X, Wang J F, Zhang L B, Bai J L, Liu Q Y, Cheng J W, Liu P Y, Li C D, Xiang J S, Ren Z A, Sun P J and Chen G F 2023 *Phys. Rev. B* **108** 205143
[9] Priolkar K R, Prabhu R B, Sarode P R, Ganesan V, Raj P and Sathyamoorthy A 1998 *J. Phys.: Condens. Matter* **10** 4413
[10] Dhar S K, Pattalwar S M and Vijayaraghavan R 1993 *Solid State Commun.* **87** 409
[11] Priolkar K R, Pattalwar S M, Mishra P K, Raj P, Sathyamoorthy A, Dhar S K, Sahni V C, Sarode P R and Prabhu R B 1997 *Solid State Commun.* **104** 71
[12] Mori H, Sato N and Sato T 1984 *Solid State Commun.* **49** 955
[13] Synoradzki K, Skokowski P, Frąckowiak Ł, Koterlyn M and Toliński T 2022 *J. Magn. Magn. Mater.* **547** 168886
[14] Priolkar K R, Rao M N, Prabhu R B, Sarode P R, Paranjpe S K, Raj P and Sathyamoorthy A 1998 *J. Magn. Magn. Mater.* **185** 375
[15] Darone GM, Hmiel B, Zhang J, Saha S, Kirshenbaum K, Greene R, Paglione J and Bobev S 2013 *J. Solid State Chem.* **201** 191
[16] Dhar S K 1994 *J. Magn. Magn. Mater.* **129** 259
[17] Moshchalkov V V, Petrenko O V and Zalyalyutdinov M K 1990 *Physica B* **163** 395
[18] Yashima H, Satoh T, Mori H, Watanabe D and Ohtsuka T 1982 *Solid State Commun.* **41** 1
[19] Umehara I, Nagai N and Ōnuki Y 1991 *J. Phys. Soc. Jpn.* **60** 1464
[20] GschneidnerJr K A, Pecharsky V K and Tsokol A O 2005 *Rep. Prog. Phys.* **68** 1479
[21] Lima Sharma A L, Bobev S and Sarrao J L 2007 *J. Magn. Magn. Mater.* **312** 400
[22] dos Reis R D, da Silva L M, dos Santos A O, Medina A M, Cardoso L P and Gandra F G 2010 *J. Phys.: Condens. Matter* **22** 486002
[23] Yashima H, Mori H, Sato N, Satoh T and Kohn K 1983 *J. Magn. Magn. Mater.* **31–34** 411
[24] Desgranges H U and Schotte K D 1982 *Phys. Lett. A* **91** 240
[25] Horn S, Holland-Moritz E, Loewenhaupt M, Steglich F, Scheuer H, Benoit A and Flouquet J 1981 *Phys. Rev. B* **23** 3171

[26] Lyu M, Wang Z, Ramesh Kumar K, Zhao H, Xiang J and Sun P 2020 *J. Appl. Phys.* **127** 193903

[27] Qiao L, Chen J, Lv B, Yang X, Wu J, Cui Y, Bai H, Li M, Li Y, Ren Z, Dai J and Xu Za 2020 *J. Alloys Compd.* **836** 155229

[28] Lyu M, Zhao H, Zhang J, Wang Z, Zhang S and Sun P 2021 *Chin. Phys. B* **30** 087101

[29] Cornut B and Coqblin B 1972 *Phys. Rev. B* **5** 4541

[30] Pikul A P, Kaczorowski D, Plackowski T, Czopnik A, Michor H, Bauer E, Hilscher G, Rogl P and Grin Y 2003 *Phys. Rev. B* **67** 224417

[31] Mondal R, Bapat R, Dhar S K and Thamizhavel A 2018 *Phys. Rev. B* **98** 115160

[32] Kondo J 1964 *Prog. Theor. Phys.* **32** 37

[33] Kumar S, Ahluwalia P K and Sharma K C 1990 *Phys. Rev. B* **41** 2030

[34] Nishida Y, Tsuruta A and Miyake K 2005 *Physica B* **359–361** 726

[35] He X, Li Y, Zeng H, Zhu Z, Tan S, Zhang Y, Cao C and Luo Y 2023 *Sci. China Phys. Mech. Astron.* **66** 237011

[36] Bauer E D, Lee H O, Sidorov V A, Kurita N, Gofryk K, Zhu J X, Ronning F, Movshovich R, Thompson J D and Park T 2010 *Phys. Rev. B* **81** 180507

[37] Szlawska M and Kaczorowski D 2011 *Phys. Rev. B* **84** 094430

[38] Rojas D P, Rodríguez Fernández J, Espeso J I, and Gómez Sal J C 2010 *J. Alloys Compd.* **502** 275

[39] Schlottmann P 1989 *Phys. Rep.* **181** 1

[40] Kaczorowski D and Ślebarski A 2010 *Phys. Rev. B* **81** 214411

[41] Cattaneo E 1986 *Z. Phys. B: Condens. Matter* **64** 305

[42] Fert A and Levy P M 1987 *Phys. Rev. B* **36** 1907